arXiv:1205.5142v1 [quant-ph] 23 May 2012

Smooth, optimal control

Florian Mintert
Freiburg Insitute for Advanced Studies, Albert-Ludwigs University of Freiburg, Albertstr. 19, 79104 Freiburg, Germany

(Dated: March 4, 2013)

This paper describes an approach to construct temporally shaped control pulses that drive a quantum system towards desired properties. A parametrization in terms of periodic functions with pre-defined frequencies results in a smooth, typically simple shape of the pulses. This enables implementation of control without broadband sources and holds the potential to improve our understanding of the functionality of optimal control.

PACS numbers: 42.50.Dv, 03.65.Yz, 02.30.Yy

Research on quantum mechanical systems is currently undergoing a process of substantial changes: whereas in the last decades the effort was mostly on the observation and description of quantum mechanical properties, currently the option to manipulate and control quantum systems is moving into focus. On the one hand, this is due to the technological advances that permit isolating quantum systems *e.g.* in ion traps [1, 2] or optical lattices [3], manipulating them coherently and letting quantum systems of different kinds interact with each other [4, 5]. On the other hand, there is the prospect to exploit intrinsically quantum mechanical properties to engineer devices with performance characteristics far beyond the classically achievable. Whereas secure communication [6] or teleportation [7] based on quantum protocols is well established by now and the possibility to simulate quantum mechanical many-body systems with quantum simulators [8, 9] is a growing field, new perspectives to exploit quantum mechanical coherence phenomena, for example in energy provision [10, 11] are just emerging.

Beyond the experimental capability to control quantum systems, any type of *quantum engineering* also needs appropriate theoretical tools that allow an experimentalist to extract optimal performance under given limitations of control, as typically imposed by power or frequency range of driving fields. Optimal control theory [12–15] provides elaborate and efficient schemes to identify *e.g.* shapes of laser or mircrowave pulses that drive a system towards desired properties. A particularly astonishing property of pulses designed by optimal control techniques is their robustness against experimental imperfections [16, 17]; for example inhomogeneous broadening in ensembles of quantum systems can be compensated essentially completely through suitably designed control pulses [18–20].

A disadvantage of these pulses is that they typically contain many frequency components; besides potential experimental challenges to generate such pulses, the complicated structure of these pulses render it essentially impossible to *understand* why they result in their astonishing performance. In particular if we want to push the envelope to large many-body systems, the answer to the question of '*why*' will become more and more important rather than the observation '*that*' one can identify suitable pulses. The aim here is therefore to strive for an approach that permits to limit a pulse to given frequency components [21], resulting in rather simple pulse shapes.

The typical scenario of optimal control theory is dynamics induced by a system- or drift-Hamiltonian $\mathcal{H}_D$ and an often time-dependent control Hamiltonian $\mathcal{H}_C(t)$. The system Hamiltonian is assumed to be inaccessible to control, *i.e.* it contains no adjustable components, whereas the control Hamiltonian can be tailored in a time-dependent fashion. The central question of interest is to determine how the propagator $\mathcal{U}$ induced by the time-dependent Hamltionian $\mathcal{H} = \mathcal{H}_D + \mathcal{H}_C(t)$ changes if the control Hamiltonian is varied, since this provides the basis for an iterative improvement of $\mathcal{H}_C(t)$ [13, 14]. Typically, the time-dependence of the control Hamiltonian stems from the time-dependence of an externally applied control field, like a laser- or microwave field, so that $\mathcal{H}_C(t) = \sum_i f_i(t)\mathcal{H}_i$, where the time-independent Hamiltonians $\mathcal{H}_i$ describe the coupling of the system to the various control fields, and $f_i(t)$ is the time-dependence of the amplitude of the corresponding field. The objects of interest thus are the functional derivatives $\delta\mathcal{U}[f_i]/\delta f_i$.

In frequently employed control algorithms like Krotov [13] and GRAPE [14, 22] the time interval in which control is exerted is divided into many short sub-intervals and the time-dependence of control fields is described by step-like pulses that are constant within each sub-interval. Consequently, the time-evolution operator $\mathcal{U}$ becomes a product of propagators for the individual sub-intervals that are induced by time-independent Hamiltonians, and the functional derivatives reduce to ordinary derivatives with respect to the fields' amplitudes in the individual sub-intervals. These ordinary derivatives can be obtained rather efficiently, which results in the astonishing performance of Krotov and GRAPE. This decomposition of the control-fields' time-dependence in piecewise constant segments, however, often results in pulse-shapes that contain high-frequency components.

In the present letter, an expansion of the field amplitudes

$$f_i(t) = \sum_j a_{ij}\ g_j(t) \tag{1}$$

in periodic functions $g_j(t)$ with a given periodicity T is employed. Since the period T can be chosen to coincide with the duration over which control is exerted, the assumption of periodicity does not result in any restriction in practice, but due to this periodicity Floquet theory [18, 21, 23] can be invoked to determine the propagator $\mathcal{U}$. According to Floquet's theorem, the Schrödinger equation with a periodically time-dependent Hamiltonian with periodicity T has a complete set of solutions

$$|\Psi_k(t)\rangle = e^{-i\varepsilon_k t}|\Phi_k(t)\rangle \tag{2}$$

with the quasi-energies ε_i and periodically time-dependent state-vectors $|\Phi_k(t)\rangle = |\Phi_k(t+T)\rangle$, which are the eigenvalues and corresponding eigenstates of the Floquet-operator $\mathcal{K} = \mathcal{H} - i\partial_t$. With the solutions given in Eq. (2) the propagator reads

$$\mathcal{U}(t) = \sum_i |\Psi_k(t)\rangle\langle\Psi_k(0)| = e^{-i\varepsilon_k t}|\Phi_k(t)\rangle\langle\Phi_k(0)| \ . \tag{3}$$

In practice, the quasi-energies ε_k and vectors $|\Phi_k(t)\rangle$ are constructed with the help of the Fourrier-transformed operator $\tilde{\mathcal{K}} = \int_0^T dt\ \mathcal{K}e^{i\omega t}/T$ of $\mathcal{K}$. $\tilde{\mathcal{K}}$ has a $2\pi/T$-periodic spectrum, and the eigenvalues ε_k and eigenvectors $|\chi_k\rangle$ within one Brillouin zone, *i.e.* interval of width $2\pi/T$ determine all solutions

$$|\Psi_k(t)\rangle = \sum_\nu |\chi_{k\nu}\rangle e^{i(\nu\omega-\varepsilon)t} \ , \tag{4}$$

of the Schrödinger equation, where $|\chi_{k\nu}\rangle$ is the subvector of $|\chi_k\rangle$ associated with the frequency component $\nu\omega$.

Since $\mathcal{U}$ is determined completely in terms of the eigensystem of $\tilde{\mathcal{K}}$ via Eqs. (3) and (4), the desired derivatives of $\mathcal{U}$ with respect to the control parameters a_{ij} are given by the corresponding derivatives of ε_k and $|\chi_k\rangle$; these, in turn, are readily obtained from a perturbative analysis of $\tilde{\mathcal{K}}$. As $\tilde{\mathcal{K}}$ depends linearly on the control parameters a_{ij}, the linear expansion

$$\tilde{\mathcal{K}} = \tilde{\mathcal{K}}_0 + \sum_{ij} \tilde{\mathcal{K}}_{ij}(a_{ij} - a_{ij}^{(0)}) \tag{5}$$

with $\tilde{\mathcal{K}}_0 = \tilde{\mathcal{K}}|_{a_{ij}=a_{ij}^{(0)}}$ and $\tilde{\mathcal{K}}_{ij} = \partial_{a_{ij}}\tilde{\mathcal{K}}$ is exact for any choice of $a_{ij}^{(0)}$. The dependence of ε_k and $|\chi_k\rangle$ on the control parameters a_{ij} can therefore be described by a series expansion with the small parameters $a_{ij} - a_{ij}^{(0)}$, and the expansion coefficients in $n-$th order are given by the $n-$th order perturbative corrections with $\tilde{\mathcal{K}}_0$ as unperturbed operator and the perturbations $\tilde{\mathcal{K}}_{ij}$. The explicit form of the derivatives reads

$$\begin{aligned}
\frac{\partial\varepsilon_k}{\partial a_{ij}} &= \langle\chi_k|\tilde{\mathcal{K}}_{ij}|\chi_k\rangle \ , \ \frac{\partial|\chi_k\rangle}{\partial a_{ij}} = -\mathcal{I}_k\mathcal{T}_{kij}|\chi_k\rangle \ , \\
\frac{\partial^2\varepsilon_k}{\partial a_{ij}\partial a_{pq}} &= -2\langle\chi_k|\mathcal{T}_{kij}\mathcal{I}_k\mathcal{T}_{kpq}|\chi_k\rangle_s \ , \\
\frac{\partial^2|\chi_k\rangle}{\partial a_{ij}\partial a_{pq}} &= 2\ \mathcal{I}_k\mathcal{T}_{kij}\mathcal{I}_k\mathcal{T}_{kpq}|\chi_k\rangle_s - \mu|\chi_k\rangle
\end{aligned}$$

where $|\chi_k\rangle$ is the eigenvector of $\tilde{\mathcal{K}}_0$ to the eigenvalue ε_k, the symbol 's' indicates symmetrization with respect to $\{i,j\}$ and $\{p,q\}$ and $\mu = \langle\chi_k|\mathcal{T}_{kij}\mathcal{I}_k^2\mathcal{T}_{kpq}|\chi_k\rangle_s$, *i.e.* $\mu = \frac{1}{2}\langle\chi_k|\mathcal{T}_{kij}\mathcal{I}_k^2\mathcal{T}_{kpq} + \mathcal{T}_{kpq}\mathcal{I}_k^2\mathcal{T}_{kij}|\chi_k\rangle$. $\mathcal{I}_k$ is the pseudo-inverse of $\tilde{\mathcal{K}}_0 - \varepsilon_k$, *i.e.* the inverse restricted to the subspace orthogonal to $|\chi_k\rangle$, and $\mathcal{T}_{kij} = \tilde{\mathcal{K}}_{ij} - \frac{\partial\varepsilon_k}{\partial a_{ij}}\mathbb{1}$.

These derivatives determine the derivatives of the propagator $\mathcal{U}$, and, in turn, of any target functional, *i.e.* property of the final state $\varrho(t_f) = \mathcal{U}(t_f)\varrho(0)\mathcal{U}^\dagger(t_f)$ at a given final time t_f that is to be optimized. Similar to Krotov and GRAPE [13, 14] this information can be used to improve a pulse sequence as parametrized by the a_i, and close-to-optimal pulses are obtained in an iterative manner.

The main goal of the present approach was to arrive at control pulses with a potentially narrow spectral range. Yet, the above expansion of a control sequence also yields various additional benefits:

- A control pulse is parametrized with comparatively few parameters; as shown below pulses with less than 10 frequency components yield very satisfactory results, whereas conventional methods with piece-wise constant functions typically require the optimization of several hundred or thousand parameters [16, 17].

- Also higher order derivatives of $\mathcal{U}$ with respect to the control fields can be obtained exactly, what improves convergence as compared to algorithms based on first derivatives only [22, 24]. The curvature is described by quadratically more scalars than the gradient, which makes its evaluation intrinsically more expensive, but due to the small number of control parameters in the present framework, accessing the exact curvature is certainly practical. If, however, this effort is to be avoided, the (scalar) curvature along a specific direction (typically the gradient) is also available in a perturbative analysis with a single perturbation $\sum_{ij} b_{ij}\tilde{\mathcal{K}}_{ij}$, where b_{ij} determines the direction along which the curvature is to be determined.

- Since the complete time-propagation operator is constructed, as opposed to its action on a predefined initial state, accessing non-linear target functionals [25] hardly requires additional effort as compared to typical functionals linear like fidelity.

- Boundary conditions, such as smooth switching on and off of the pulses, can be realized easily through a suitable paramterization in Eq.(1).

- Since all dynamics are given by time-dependent exponential functions, which can be integrated analytically, time-averaged target functionals can also be implemented without additional overhead. This permits, for example to minimize the deviation from a desired dynamics over a finite time-interval.

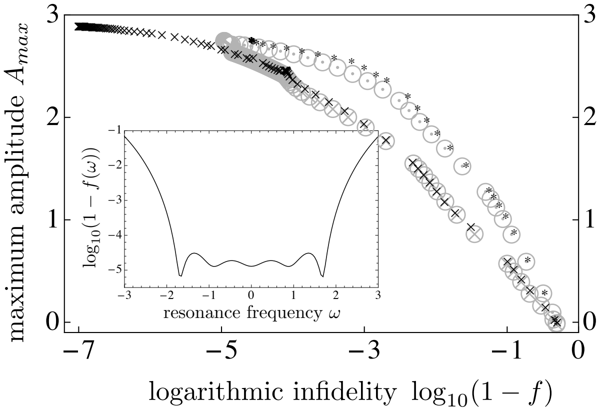

FIG. 1: Logarithmic infidelity and required maximal amplitude as obtained via 100 steps of iteration for spin ensembles with frequency range $2 \geq \omega \geq -2$ ($1 \geq \omega \geq -1$) depicted in grey (black) and $i_{max} = 4(7)$ components in the control pulse depicted with $*$, $\odot$ ($\times$, $\odot$). The inset show the logarithmic infidelity achieved with the pulse after 100 iterations as function of the resonance frequency of the spin in Eq. (6). This pulse with $a_1 = 0.498$ $a_2 = -1.904$ $a_3 = 2.114$ $a_4 = 0.884$ has been constructed to achieve close-to-unit fidelity in the interval $2 \geq \omega \geq -2$.

Having established the framework, its efficiency can be demonstrated with the paradigmatic example of an inhomogeneously broadened spin-ensemble. Each spin is described by the Hamiltonian

$$\mathcal{H}_\omega = \frac{\omega}{2}\sigma_z + A(t)\sigma_y \text{ with } A(t) = \sin t\,(\sum_{i=1}^{i_{max}} a_i \sin it), \quad (6)$$

with its natural eigenfrequency ω. All units are taken in terms of the natural system frequency so that the scaled frequency ω, $A(t)$, a_i and t are unitless. The pulse-shape given in terms of the prefactors a_i are to be determined and the parametrization ensures that the control-pulse and its time-derivative vanish at $t = 0$ and $t = \pi$ when the control field is switched on and off. The goal is to drive a transition from the σ_z eigenstate $|1\rangle$ to the balanced superpositions $|\Phi\rangle = (|0\rangle + |1\rangle)/\sqrt{2}$ of both σ_z eigenstates. The pulse should achieve this goal for a broad range of system eigen-frequencies ω. This can be achieved with the help of an ensemble of spins described by Eq. (6) with different frequencies ω and the requirement that the pulse realize the desired dynamics for each ensemble member. In the present case, an ensemble of 50 spins with ω drawn from a uniform distribution from the interval $[-2, 2]$ was used. Choosing an interval centered at 0 implies a transformation to an interaction picture, where the average spin is stationary and the part of the driving field that oscillates with twice the average resonance frequency can be neglected [27].

Target of control is the averaged fidelity $\bar{f} = \langle f(\omega)\rangle_\omega$, where $f(\omega) = |\langle\Psi_\omega|\Phi\rangle|^2$ is the fidelity between the final state $|\Psi_\omega\rangle$ that is reached with the Hamiltonian $\mathcal{H}_\omega$ and the average in $\bar{f}$ is taken over the considered ensemble. To ensure the identification of a pulse with low intensity, there is an additional penalty function that creates an incentive to find weak pulses. Specifically, it reads $\mathcal{F} = \bar{f} - p\int_0^{t_f} dt A^2$ with a non-negative function p that decreases as the algorithm reaches its target. The inset of Fig. (1) depicts the infidelity $1 - f_\omega$ for a pulse with $i_{max} = 4$ components obtained after 100 iterations. The logarithmic scale indicates that a fidelity of $f(\omega) \simeq 99.999\%$ has been reached in the entire interval $2 \geq \omega \geq -2$.

The lowest order term $a_1 \simeq 1/2$ corresponds to a pulse that achieves the desired dynamics for a spin with $\omega = 0$. A pulse with only this component has a maximal amplitude of $1/2$ at $t = t_f/2$. The higher order components a_i ($i > 1$) that achieve the robustness of the pulse under variations of ω necessarily lead to higher amplitudes, so that the numerically obtained pulse has a maximum amplitude of 2.77 that is attained at $t = 0.717\ t_f$. The prize for the robustness is thus an increase of maximum amplitude by a factor of 5.5.

Fig. 1 depicts the performance in terms of logarithmic infidelity and maximum amplitude of the pulses obtained during the iteration. To start with, the pulse is initialized randomly with very weak amplitude, and Fig. 1 shows how the obtained fidelity increases with growing amplitude. The symbol '$\times$' in Fig. 1 correspond to the case with spread of resonance frequencies $2 \geq \omega \geq -2$ discussed above. The symbol '$*$' correspond to $1 \geq \omega \geq -1$; not surprisingly, a given fidelity can be reached with lower amplitudes than in the former case, and larger fidelities (up to $1 - 10^{-7}$) can be reached. On the other hand, the performance does *not* improve if more higher frequency components are included in the control pulse as depicted with the symbols '$\odot$' and '$\otimes$' that correspond to pulses with $i_{max} = 7$ in Eq. (6). As it can be seen, the amplitude-fidelity characteristic coincides with that of the $i_{max} = 4$ case. That is, there is no improvement in going to broader frequency ranges, but only a slight decrease in the rate of convergence.

To gain insight into the dynamics of the spin ensemble, it is instructive to inspect three components of the Bloch vector, *i.e.* $\langle 1|\mathcal{U}^\dagger(t)\sigma_i\mathcal{U}(t)|1\rangle$ ($i = x, y, z$) with the Pauli matrices σ_i. They are displayed in Fig. (2) for 200 spins with resonance frequencies in the interval $5 \geq \omega \geq -5$. The trajectories corresponding the spins in the interval $2 \geq \omega \geq -2$ for which the pulse had been designed are depicted in black; the other trajectories are depicted in grey. As it can be seen, during the course of time the trajectories spread, but there are several instances when the individual components of the black trajectories are refocussed. There are two such events during the propagation for the σ_x-component and one rather weak focus for the σ_y component. Only at the end of the propagation at $t = t_f$ are all the three components refocussed. The grey trajectories often deviate strongly from the black ones, and, in particular, at t_f when the black ones are being

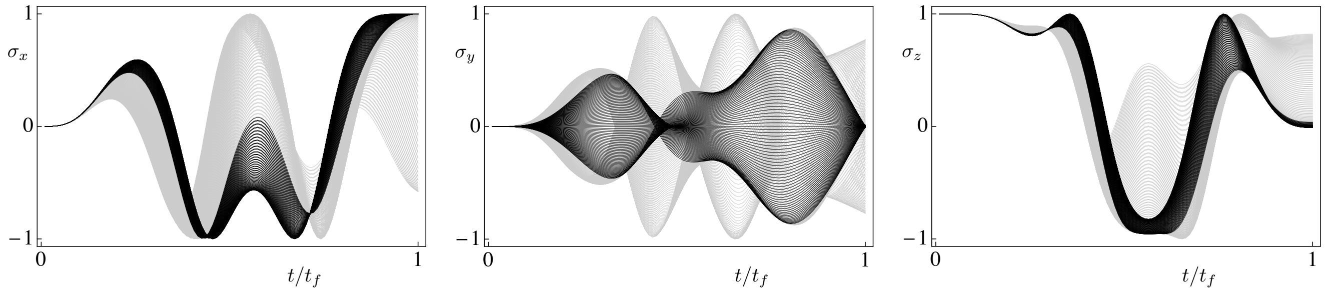

FIG. 2: Dynamics of spin components for 500 spins. The gray trajectories correspond to spins with resonance frequencies outside the targeted frequency window; the black trajectories correspond to the frequency range within which the desired target state is to be achieved.

strongly refocussed, the grey ones rather spread strongly.

Whereas the focus here was on the coherent dynamics of an ensemble of non-interacting spins the present approach directly applies also to interacting manybody systems, and it can also be extended to dissipative quantum systems [26]. In particular, in the growing field of hybrid quantum systems the present method opens up new pathways to control the interaction between components of different types, improve coherence or entanglement properties, or also, *e.g.* to improve the accuracy in the identification of system properties.

Acknowledgment Stimulating discussion with Steffen Glaser, Simeon Sauer, Fabian Bohnet-Waldraff, Andreas Buchleitner and Johannes Majer and financial support by the European Research Council are gratefully acknowledged.

[1] H. Häffner, C. Roos, and R. Blatt, Phys. Rep. **496**, 155 (2008).
[2] R. Blatt and D. Wineland, Nature **453**, 1008 (2008).
[3] I. Bloch, J. Dalibard, and W. Zwerger, Rev. Mod. Phys. **80**, 885 (2008).
[4] L. Childress, M. V. Gurudev Dutt, J. M. Taylor, A. S. Zibrov, F. Jelezko, J. Wrachtrup, P. R. Hemmer, and M. D. Lukin, Science **314**, 281 (2006).
[5] A. C. Bleszynski-Jayich, W. E. Shanks, B. Peaudecerf, E. Ginossar, F. von Oppen, L. Glazman, and J. G. E. Harris, Science **326**, 272 (2009).
[6] C. Kurtsiefer, P. Zarda, M. Halder, H. Weinfurter, P. Gorman, P. Tapster, and J. Rarity, Nature **419**, 450 (2002).
[7] I. Marcikic, H. de Riedmatten, W. Tittel, H. Zbinden, and N. Gisin, Nature **421**, 509 (2003).
[8] A. Friedenauer, H. Schmitz, J. T. Glueckert, D. Porras, and T. Schaetz, Nat. Phys. **4**, 757 (2008).
[9] J. Struck, C. Ölschläger, R. Le Targat, P. Soltan-Panahi, A. Eckardt, M. Lewenstein, P. Windpassinger, and K. Sengstock, Science **333**, 996 (2011).
[10] G. Engel, T. Calhoun, E. Read, T.-K. Ahn, T. Mancal, Y.-C. Cheng, R. Blankenship, and G. Fleming, Nature **446**, 782 (2007).
[11] E. Collini, C. Y. Wong, K. E. Wilk, P. M. G. Curmi, P. Brumer, and G. D. Scholes, Nature **463**, 644 (2010).
[12] D. D'Alessandro, *Introduction to quantum control and dynamics* (CRC Press, 2007).
[13] *Global Methods in Optimal Control Theory* (Marcel Dekker, New York, 1996).
[14] N. Khaneja, T. Reiss, C. Kehlet, T. Schulte-Herbrüggen, and S. J. Glaser, J. Mag. Res. **172**, 296 (2005).
[15] C. Brif, R. Chakrabarti, and H. Rabitz, New Journal of Physics **12**, 075008 (2010).
[16] B. Schneider, C. Gollub, K.-L. Kompa, and R. de Vivie-Riedle, Chemical Physics **338**, 291 (2007).
[17] T. Hornung, M. Motzkus, and R. de Vivie-Riedle, Phys. Rev. A **65**, 021403 (2002).
[18] G. Goelman, S. Vega, and D. B. Zax, Phys. Rev. A **39**, 5725 (1989).
[19] D. Abramovich and S. Vega, Journal of Magnetic Resonance, Series A **105**, 30 (1993).
[20] T. E. Skinner, K. Kobzar, B. Luy, R. Bendall, W. Bermel, N. Khaneja, and S. J. Glaser, J. Magn. Reson. **179**, 241 (2006).
[21] T. E. Skinner and N. I. Gershenzon, Journal of Magnetic Resonance **204**, 248 (2010).
[22] P. de Fouquieres, S. Schirmer, S. Glaser, and I. Kuprov, arxiv:1102.4096.
[23] G. Floquet, Ann. École Norm. Sup. **12**, 47 (1883).
[24] P. de Fouquieres, arXiv:1202.2530.
[25] F. Platzer, F. Mintert, and A. Buchleitner, Phys. Rev. Lett. **105**, 020501 (2010).
[26] R. Blümel, A. Buchleitner, R. Graham, L. Sirko, U. Smilansky, and H. Walther, Phys. Rev. A **44**, 4521 (1991).
[27] This rotating wave approximation is valid if the actual resonance frequency is large compared to the control amplitude $A(t)$ and the spread of resonance frequencies in the ensemble.